Unveiling nonperturbative factors in the resonant photoionization time delay

Xiao-Yun Zhao(赵晓云)[1,2] and Ming-Qing Liu (刘明清)[3*]

[1]School of Physics and Electrical Engineering, Weinan Normal University, Weinan 714099, China

[2]Engineering Research Center of X-ray Imaging and Detection, University of Shaanxi Province, China

[3]School of Physics and Information Technology, Shaanxi Normal University, Xi'an 710119, China

August 12, 2026

Abstract

Atomic photoionization time delay is a vital component of attosecond metrology for investigating the ultrafast electron dynamics in atomic systems on their natural time scale. Here, we probe the factor which leads to the nonperturbative characteristics of resonant photoionization time delay (RPTD) of atomic hydrogen by numerically solving the time-dependent Schrödinger equation (TDSE) and the strong-field nonperturbation theory (SFNPT) with considering the population depletion and ac-Stark energy shift of ground state. RPTD can be retrieved from the energy-resolved optical phase of a bicircular two-color field corresponding to the maximal asymmetry of photoelectron angular distribution even in the nonperturbative regime. Our results reveal that as laser intensity increases the RPTD shows a remarkable difference of energy-dependent behaviors. At lower intensity, the absolute value of RPTD displays a smooth drop with increasing electron energy, however, at higher intensity its absolute value exhibits an obvious enhancement. Given the agreement between TDSE and SFNPT, we clearly elucidate the physical origin of nonperturbative characteristics, i.e., the population depletion of ground state plays a crucial role rather than ac-Stark energy shift. More specifically, the population depletion severely affects the Fourier transformation of the laser envelope, which is an important phase component of transition amplitude. Our work clarifies the physical mechanism of atomic photoionization time delay in nonperturbative environments, advancing the comprehensive understanding of time in attosecond science.

Keywords: photoionization time delay, nonperturbative characteristics, photoelectron angular distributions, bicircular two-color interferometry

PACS: 42.50.Hz, 32.80.Rm, 32.80.Qk

*Corresponding author. E-mail:mingqing.liu@snnu.edu.cn

1. Introduction

Photoionization—the ejection of an electron from an atom upon photon absorption—ranks among the most fundamental quantum phenomena [1,2]. In the nonresonant regime, the outgoing wave packet is commonly assumed to respond to the incident field instantaneously. In the 1950s [3,4], the possibility of a delayed response was recognized, which is generally called Wigner time delay [5] that is characterized by a slight temporal offset in the release of the photoelectron wave packet upon absorption of a short electromagnetic pulse by an atom [6–11]. However, time in the quantum world is not a physical quantity that can be directly observed due to the lack of the corresponding time operator in quantum mechanics. Nevertheless, one can design various schemes with different configurations of weak extreme ultraviolet (XUV) pulse and infrared pulse (IR) to extract temporal information from the energy-resolved photoionization signals, such as attosecond streaking [12–14] and RABBITT [15,16]. In addition, a two-color interferometric method is proposed to retrieve the time delay between one- and two-photon ionization from the asymmetry in the photoelectron angular distributions without scanning XUV-IR delay [17,18], which can be obtained by taking the derivative of the energy with respect to the scattering phase shift during electron transitions in the continuum [19,20].

In the presence of a resonance, the photoelectron propagation is naturally delayed relative to the free space propagation. Thus the Wigner time delay acquires large positive values in hundreds of attoseconds range (1 as $= 10^{-18}$ s). The RABBITT technique has also allowed for the time resolution of Fano resonances [21]. In this case, resonant photoionization time delay (RPTD) is generally regarded as the period in which electrons are temporarily trapped in a resonant state [22–24]. How to retrieve the intermediate-excited-state-assisted RPTD is an important issue in attosecond physics [25]. However, most current experimental and theoretical studies on RPTD are in the perturbative regime due to the moderate intensity and high photon energy of XUV pulses, in which time-dependent perturbation theory (PT) [26] can well reproduce the numerical resolution of the time-dependent Schrödinger equation (TDSE) [16,27]. Up to now, isolated attosecond pulses (IAPs) originated from XUV radiation with photon energy of 20–45 eV and duration of 180 as are experimentally available [28]. However, for such ultrashort duration, the intensity of the XUV pulse is lower than 10^{12} W/cm^2. In Ref. [29], Richter *et al.* have already experimentally employed XUV pulse with intensity reaching 2.9×10^{14} W/cm^2, photon energies around 21 eV, but pulse duration is as long as 49 fs. The primary challenge lies in balancing the contradiction between enhancement of intensity and reduction of pulse width. With the continuous advancement of laser technology, the aforementioned contradiction will inevitably be resolved in the future [30].

As the intensity of laser pulse increases further, strong resonance between the ground state and the first excited state induces the population depletion and Stark energy shift of the ground state [31–33], leading to that the standard perturbation theory is not suitable for describing the ionization process. However, research on the nonperturbative RPTD and its properties still remain scarce. Recently, we develop a strong-field nonperturbation theory (SFNPT) by taking the population depletion and Stark energy shift of the ground state into account [34], which shows a good agreement with the TDSE, to better retrieve the RPTD in the nonperturbation regime by using a bicircular two-color interferometry. For the higher intensity, the two strong-field factors, i.e., the population depletion and Stark energy shift of the ground state, not only affect the magnitude of the transition amplitude, but also significantly change its phase, thereby influencing the derivative of the phase with respect to energy. Hence, to figure out which strong-field factor dominates in shaping the nonperturbative features of RPTD contributes to a comprehensive understanding of the physical mechanism behind the formation of RPTD in the nonperturbative regime.

In this work, we represent a theoretical investigation on the intensity dependence of RPTD in hydrogen atoms by using counter-rotating ω-2ω circularly polarized XUV laser pulses, that is, bicircular two-color interferometry. The ground state resonantly couples to the excited state by the absorption of a right-handed circularly polarized (RCP) photon of frequency ω, followed by subsequent absorption of the same photon, promoting this excited state to a continuum state. This continuum state coherently interferes with the scattering state generated by absorbing one left-handed circularly polarized (LCP) photon of frequency 2ω from the ground state. The time delay induced by one-photon absorption is insensitive to the rotation direction of the circularly polarized XUV pulse, resulting in the

RPTD being approximately treated as a time delay between the one- and two-photon ionization pathways. The interference between these two ionization pathways results in asymmetry in the angular distribution of photoelectrons. By adjusting the relative optical phase of the two-color field, we first retrieve the energy-dependent RPTD as intensity increases from the relative optical phase corresponding to the maximal asymmetry. Then, we study the physical picture underlying nonperturbative features of the energy-dependent RPTD by taking the advantages of the SFNPT model that the roles of ground-state depletion and Stark energy shift can be disentangled. Based on the analysis of SFNPT model, we elaborate the population depletion of ground state plays a dominant role in shaping the nonperturbative features of RPTD. Our works can spur the further experiment to explore the nonperturbative characteristics of time delay and demonstrate the physical mechanisms behind nonperturbative features of RPTD.

2. Theoretical framework

2.1. TDSE simulations

The dynamics of a hydrogen atom interacting with the counter-rotating two-color circularly polarized laser fields is governed by the 3D-TDSE, which reads (atomic units are used unless otherwise stated)

$$i\frac{\partial}{\partial t}\Psi(\mathbf{r},t)=\left[-\frac{\nabla^2}{2}-\frac{1}{r}-i\mathbf{A}(t,\phi)\cdot\nabla\right]\Psi(\mathbf{r},t), \quad (1)$$

in the reduced-velocity gauge. The vector potential is described as

$$\mathbf{A}(t,\phi)=\mathbf{A}_R(t,\omega,0)+\mathbf{A}_L(t-\tau,2\omega,\phi), \quad (2)$$

$\mathbf{A}_R(t)$ and $\mathbf{A}_L(t)$ describe the vector potential of RCP and LCP laser pulses, respectively, and ϕ and τ are the optical phase difference and time delay of two-color field, respectively. In our calculations, both pulses propagate along the z axis and are polarized in the xOy plane. The expressions of the vector potential for the RCP and LCP laser pulses are written as

$$\mathbf{A}_{R,L}(t,\omega,\phi)=\frac{A_0 f(t)}{\sqrt{2}}[\cos(\omega t+\phi)\hat{\mathbf{e_x}}\pm\sin(\omega t+\phi)\hat{\mathbf{e_y}}], \quad (3)$$

where "+" and "−" indicate the RCP and LCP laser pulses. Here, $\hat{\mathbf{e_x}}$ and $\hat{\mathbf{e_y}}$ are the unit vectors along the x and y axes. $A_0=\mathcal{E}_0/\omega$ denotes the amplitude of the vector potential. ω is the central angular frequency of the laser field. $\mathcal{E}_0=\sqrt{I_0/I_{\rm AU}}$ is the amplitude of the electric field. I_0 is the peak laser intensity, and $I_{\rm AU}\approx 3.51\times10^{16}$ W/cm^2 is the atomic unit of laser intensity. In our simulations, each pulse has a temporal envelope $f(t)=\cos^2(\frac{\pi t}{T})$ with $-T/2\le t\le T/2$, T is the pulse duration. Time delay of two pulses τ is chosen as 4 fs in order to completely separate the two pulses, guaranteeing that the two-photon ionization occurs prior to the arrival of the second pulse. 10 optical cycles are used for respective pulse and the frequency $\omega=10$ eV, which can boost the resonance of the initial state $1s$ and the excited $2p$ state (with $m=1$ or -1) of the hydrogen atom. Hence, $T=4.14$ fs for the first pulse and $T=2.07$ fs for the second pulse. $I_0\equiv I_\omega=10I_{2\omega}$, according to a general experimental observations that the intensity of second-harmonic light is lower than that of the fundamental frequency light [35].

The wave function $\Psi(\mathbf{r},t)$ of the 3D-TDSE in Eq. (1) is expanded by spherical harmonics $Y_{lm}(\theta,\varphi)$ with polar angle θ and azimuthal angle φ, where l and m are the angular momentum quantum number and the magnetic quantum number, respectively. The radial part of the wave function is treated with the finite-element discrete variable representation (FE-DVR) method [36]. The initial wave function is prepared by the imaginary-time propagation. The time propagation of the electron wave function $\Psi(\mathbf{r},t)$ is implemented by the split-Lanczos method [37], which greatly improves the efficiency of the traditional Lanczos propagator by splitting out the centrifugal potential from the Hamiltonian. To avoid the use of very large radial box, the wave-splitting technique [38] is adopted. According to the wave-splitting technology, at the end time t_f of the propagation, we obtain the final ionization amplitude $\rho(\mathbf{k},t_f)$ by adding all the amplitudes at time t_f. In the polarization plane, the differential ionization probability $P(E,\theta=\frac{\pi}{2},\varphi)=k|\rho(k,\theta=\frac{\pi}{2},\varphi,t_f)|^2$. The asymmetry in the photoelectron angular distributions is defined as

$$\alpha(E)=\frac{\int_0^\pi P(E,\varphi)d\varphi-\int_\pi^{2\pi}P(E,\varphi)d\varphi}{\int_0^\pi P(E,\varphi)d\varphi+\int_\pi^{2\pi}P(E,\varphi)d\varphi}, \quad (4)$$

which gives the difference of electron yield emitted into opposite sides of the plane parallel to the light polarization. As shown below, we can extract the RPTD from maximal asymmetry in photoelectron angular distributions .

In our calculations, a time step $\Delta t=0.01$ a.u. for the time propagation of the electron wave func-

tion, the maximal box size for radial coordinates is set to $R_{\max} = 400$ a.u., and the absorbing boundary is $R_c = 240$ a.u., the number of finite-element is 400 and 8 basis functions is set for each finite-element. In addition, the maximal numbers of the angular momentum quantum ($\ell_{\max}$) and the magnetic quantum ($m_{\max}$) are both set to be 12. The convergence of our calculations is confirmed by changing these parameters.

2.2. Strong-field non-perturbative theory (SFNPT)

If the resonance between ground state and excited state occurs, the nonperturbative effects such as the population depletion and ac-Stark energy shift of initial state should be considered. The transition amplitude of one-photon ionization is given by

$$\mathcal{A}_1(\mathbf{k}) = -i\int_{t_0}^{t_f}\langle\Psi_{\mathbf{k}}|\mathbf{r}\cdot\vec{\mathcal{E}}(t)|\Psi_i\rangle e^{iEt}s_0(t)dt, \quad (5)$$

where $|\Psi_{\mathbf{k}}\rangle$ is the final scattering state with asymptotic momentum $\mathbf{k}$, photoelectron energy $E = k^2/2$, and $|\Psi_i\rangle$ is the initial ground state with energy $E_i = -13.6$ eV. $t_0 = -T/2$ and $t_f = \tau + T/2$. The electric field $\vec{\mathcal{E}}(t) = \frac{\mathcal{E}_0}{\sqrt{2}}f(t)[\sin(\omega t+\phi)\hat{\mathbf{e}_x} \mp \cos(\omega t+\phi)\hat{\mathbf{e}_y}]$, where $\mathcal{E}_0 = A_0\omega$ is the peak intensity of electric field. $s_0(t)$ is the amplitude of the initial state at t. The occupation amplitude $s_0(t)$ includes the depletion of population as well as the Stark energy shift of the initial state,

$$s_0(t) = g(t)\exp\left[-i\left(E_i t + \int_{-T/2}^{t}\delta E_i(\tau')d\tau'\right)\right] \quad (6)$$

with $g(t)$ the modulus of $s_0(t)$ and $\delta E_i(\tau')$ the instantaneous energy shift induced by the XUV pulse.

The interaction operator $\mathbf{r}\cdot\vec{\mathcal{E}}(t)$ in the rotating wave approximation (RWA) can be written as

$$\begin{aligned}\mathbf{r}\cdot\vec{\mathcal{E}}(t) =& \frac{i\mathcal{E}_0}{2\sqrt{2}}\{f(t)e^{-i\omega t}(x+iy)\\ &+ f(t-\tau)e^{-i2\omega(t-\tau)}e^{-i\phi}(x\mp iy)\},\end{aligned} \quad (7)$$

where "+" and "−" indicate the co-rotating and counter-rotating pulse configurations, respectively. The two terms in Eq. (7) denote the absorption process of one ω-photon and one 2ω-photon, respectively. Substituting Eq. (7) into Eq. (5), the amplitude $\mathcal{A}_1$ can be rewritten as

$$\begin{aligned}\mathcal{A}_1(\mathbf{k}) =& \frac{\mathcal{E}_0}{2\sqrt{2}}\{\langle\Psi_k|x+iy|\Psi_i\rangle\hat{\mathcal{F}}(E-\omega)\\ &+ \langle\Psi_k|x\mp iy|\Psi_i\rangle e^{-i\phi}\hat{\mathcal{F}}(E-2\omega)\},\end{aligned} \quad (8)$$

where the Fourier transform of the product of pulse envelope and the occupation amplitude of initial state

$$\hat{\mathcal{F}}(E-n\omega) = \int_{-T/2}^{T/2}e^{i(E-n\omega)t}f(t)s_0(t)dt, \quad n = 1, 2. \quad (9)$$

It can be easily seen from Eq. (8) that the one-photon transition amplitude phase is contributed by the radial dipole matrix element and the Fourier transform of the pulse envelope. Obviously, the transition phase from the radial dipole matrix element is independent of laser intensity.

To explicitly show the intensity dependence of transition amplitude phase, the Fourier transform of the pulse envelope can be rewritten as

$$\hat{\mathcal{F}}(E-n\omega) = \int_{-T/2}^{T/2}\{\cos[h(t)] + i\sin[h(t)]\}f(t)g(t)dt, \quad (10)$$

where

$$h(t) = (E - E_i - n\omega)t - \int_{-T/2}^{t}\delta E_i(\tau')d\tau'. \quad (11)$$

If the depletion of population and Stark shift of initial state are ignored, i.e., $g(t) = 1$ and $\delta E_i(\tau') = 0$, then the conventional transition amplitude in lowest-order PT would be recovered, and the time integration over $(-T/2, T/2)$ of the imaginary part of Eq. (10) is zero due to $\sin[(E - E_i - n\omega)t]f(t)$ is an odd function. Thus, Eq. (10) can be rewritten as $\int_{-T/2}^{T/2}\cos[(E - E_i - n\omega)t]f(t)dt$, which is a positive real and intensity-independent number. Hence, in perturbative regime, the one-photon transition amplitude phase can be regard as intensity-independent number. However, in deep nonperturbative regime, intensity dependence of $g(t)$ and $\delta E_i(\tau')$ results in the imaginary part of Eq. (10) not zero, leading to the intensity dependence of transition amplitude phases.

The second-order transition amplitude in SFNPT is given by

$$\begin{aligned}\mathcal{A}_2(\mathbf{k}) = -\sum_{q\neq i}\int_{t_0}^{t_f}&\langle\Psi_{\mathbf{k}}|\mathbf{r}\cdot\vec{\mathcal{E}}(t)|\Psi_q\rangle e^{i(E-E_q)t}\\ &\times\int_{t_0}^{t}\langle\Psi_q|\mathbf{r}\cdot\vec{\mathcal{E}}(t')|\Psi_i\rangle e^{iE_qt'}s_0(t')dt'dt,\end{aligned} \quad (12)$$

where $|\Psi_q\rangle$ with energy E_q is the intermediate state, and the index q denotes all intermediate states including bound and continuum states. Note that in this work the two-photon ionization does not involve the absorption of 2ω photon, i.e. the second term in Eq. (7) can be omitted. Therefore, Eq. (12) can be rewritten

as

$$\mathcal{A}_2(\mathbf{k}) = \frac{\mathcal{E}_0^2}{8}\sum_{q\neq i}\langle\Psi_\mathbf{k}|x+iy|\Psi_q\rangle\langle\Psi_q|x+iy|\Psi_i\rangle\Pi_q(E) \tag{13}$$

where

$$\Pi_q(E) = \int_{-T/2}^{T/2} e^{i(E-E_q-\omega)t} f(t)dt \times \int_{-T/2}^{t} e^{i(E_q-\omega)t'} f(t')s_0(t')dt'. \tag{14}$$

$\Pi_q(E)$ indicates the Fourier transform of the laser pulse envelope $f(t)$ with the correction of initial state, which is a complex number. If the depletion of population and Stark shift of initial state are ignored, i.e., $s_0(t') = e^{-iE_it'}$, the conventional transition amplitude in 2nd-order PT would be recovered. If we only consider the depletion of population, then $s_0(t') = g(t')e^{-iE_it'}$. Note that the time-dependent $g(t)$ and $\delta E_i(t)$ can be obtained directly from TDSE simulations.

In our SFNPT calculations, the wave functions of initial state and each intermediate eigenstate are obtained by the diagonalization of free-field Hamiltonian, which is discretized using the FE-DVR representation method. In the calculation of two-photon amplitude, the radial box size of $R_{\max} = 50$ a.u., the first 100 intermediate eigenstates (including bound and continuum states) are chosen within the total 300 intermediate eigenstates, which already make sure the convergence of calculation. The numbers of finite element and basis functions are 50 and 7, respectively.

2.3. Retrieving RPTD from the asymmetry in photoelectron angular distributions

According the electric dipole selection rules and RWA, the ground state $1s$ with $m = 0$ [denoted by $(s, 0)$] by absorbing one LCP photon creates a continuum wave $(p, -1)$ at the energy $E_k = 2\omega + E_i$ with angular distribution $\sim Y_{1-1}(\theta, \varphi)$. The same energy can be reached via a two-photon absorption from the RCP pulse, the angular dependence of the continuum wave $(d, 2)$ populated by the two-photon path is $Y_{22}(\theta, \varphi)$.

The angle-resolved ionization probability can be written as

$$P(E, \varphi) = k|\mathcal{M}_{p,-1}(\mathbf{k}) + \mathcal{M}_{d,2}(\mathbf{k})|^2, \tag{15}$$

where the transition amplitude of each partial wave can be expressed by [18]

$$\mathcal{M}_{p,-1}(\mathbf{k}) = a_{1,-1}e^{is_{1,-1}}e^{i(E-E_i)\tau}e^{-i\phi}Y_{1-1}, \tag{16}$$

$$\mathcal{M}_{d,2}(\mathbf{k}) = a_{2,2}e^{is_{2,2}}Y_{22}, \tag{17}$$

where $a_{1,-1}$ and $a_{2,2}$ are the real-value partial wave amplitudes, $s_{1,-1}$ and $s_{2,2}$ are the corresponding arguments. $\mathcal{M}_{p,-1}$ and $\mathcal{M}_{d,2}$ are calculated by Eq. (8) and Eq. (13), respectively. Therefore, the energy-resolved asymmetry $\alpha(E)$ defined by Eq. (4) in the polarization plane ($\theta = \pi/2$) can be rewritten as

$$\alpha(E) = -\beta\sin[\phi - (s_{1,-1} - s_{2,2}) - (E - E_i)\tau], \tag{18}$$

where the parameters $\beta = \sqrt{5}/(4\pi^2 Q)a_{1,-1}a_{2,2}$, $Q = (a_{1,1}|Y_{1-1}|)^2 + (a_{2,2}|Y_{22}|)^2$. In the counter-rotating case, we have checked that $a_{1,-1}$, $a_{2,2}$, $s_{1,-1}$ and $s_{2,2}$ are independent of ϕ. ϕ_m (the relative phase corresponding to the maximal asymmetry) yields

$$\phi_\mathrm{m} - (s_{1,-1} - s_{2,2}) - (E - E_i)\tau = -\frac{\pi}{2} + n\cdot 2\pi, \tag{19}$$

where n is an integer number. As a result, the phase difference between one- and two-photon ionization amplitudes

$$\Delta\Phi = \phi_\mathrm{m} - (E - E_i)\tau + \frac{\pi}{2} + n\cdot 2\pi, \tag{20}$$

where $\Delta\Phi = s_{1,-1} - s_{2,2}$ denotes the phase difference between one- and two-photon ionization pathways. ϕ_m can be extracted from the energy-resolved asymmetry in photoelectron angular distributions. Therefore, the time delay between one- and two-photon ionizations

$$\tau_\mathrm{R} = d\Delta\Phi/dE = d\phi_\mathrm{m}/dE - \tau, \tag{21}$$

which indicates that the RPTD equals to the energy derivative of the ϕ_m subtracts the delay between the two pulses.

3. Results and discussions

Figure 1 shows the time delay between one- and two-photon ionization pathways τ_R obtained by the retrieval procedure as illustrated above, i.e., the time difference forming p- and d- partial waves. Since the ionization probability of above-threshold-ionization peaks is too small, we will only discuss the features around electron energy $E = 2\omega + E_i = 6.4$ eV where the ionization signals are strongest. It can be seen that all time delays are negative, indicating that the photoelectrons ionized through the single-photon ionization pathway arrive at the scattering state earlier than

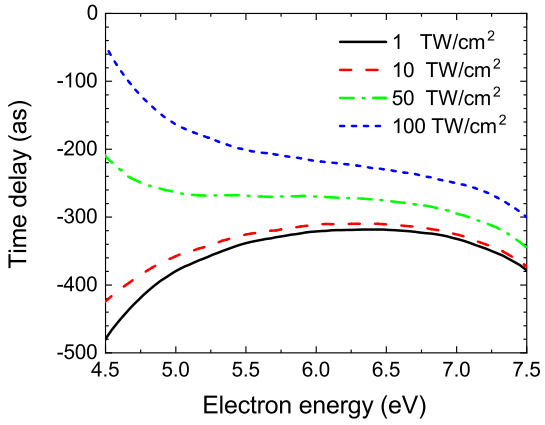


Fig. 1. Time delay between one- and two-photon ionizations calculated by TDSE as a function of electron energy at four different laser peak intensities: 1, 10, 50, and 100 TW/cm^2.

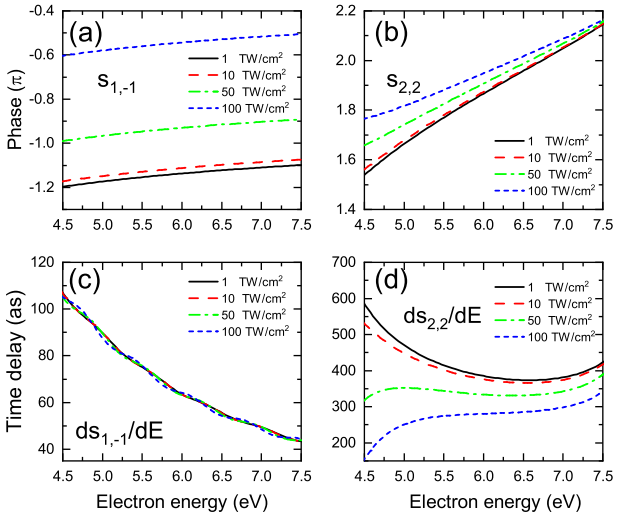


Fig. 2. One-photon amplitude phase $s_{1,-1}$ (a) and two-photon amplitude phase $s_{2,2}$ (b) as a function of electron energy obtained by TDSE calculations and their derivative with respect to the energy $ds_{1,-1}/dE$ (c) and $ds_{2,2}/dE$ (d).

those of the same energy, but are ionized via the two-photon ionization pathway. This time difference in current laser parameters τ_R can be regarded as RPTD, as demonstrated in our previous work [34]. The magnitude of RPTD is on the order of hundreds of attoseconds, which is consistent with Ref. [39]. Furthermore, the absolute values of time delays at low-intensity pulse are larger than those at high-intensity pulse, which indicates that the bound excited states are more easily ionized by higher-intensity pulses.

As shown by Fig. 1, at lower intensities (such as 1 and 10 TW/cm^2), the absolute value of time delay displays a decrease trend (perturbative regime). However, at higher intensities (such as 50 and 100 TW/cm^2), the absolute value of time delay consistently increases with increasing energy (nonperturbative regime), which represents the most pronounced distinguishing characteristic of time delays in perturbative and nonperturbative regimes. As the intensity increases, the resonance between the ground state and the $2p$ excited state becomes stronger. This resonance has a more pronounced effect on low-energy electrons.

To figure out the physical mechanism underlying this difference of RPTD induced by the laser intensity, we separately examine the amplitude phase of single- and two-photon ionization, i.e., $s_{1,-1}$ and $s_{2,2}$, as well as their respective derivatives with respect to energy due to the relation $\tau_R = d(s_{1,-1} - s_{2,2})/dE$, as shown by Fig. 2. It can be seen that the single-photon ionization phase $s_{1,-1}$ is not very sensitive to the electron energy, which shows a slow and smooth rise with increasing energy [Fig. 2(a)], however, the two-photon ionization phase $s_{2,2}$ displays a rapidly growth [Fig. 2(b)]. For the intensity dependence of phase, as laser intensity increases, $s_{1,-1}$ increases significantly overall, but the increment is roughly the same for each energy, which leads to its derivative with respect to energy being insensitive to the variation of intensity, as depicted in Fig. 2(c). For two-photon ionization phase, $s_{2,2}$ also shows an overall increase, but it is less pronounced compared to $s_{1,-1}$, and the increment is more significant at low energies. Therefore, this characteristic strongly affects the dependence of its energy derivative on intensity. As shown by Fig. 2(d), at lower intensities $ds_{2,2}/dE$ shows an overall drop while at higher intensities it presents an obvious increase for low-energy electrons. Of course, this intensity-induced difference is more pronounced for low-energy electrons, which is consistent with the phenomenon in Fig. 1. By comparing Fig. 1 and Fig. 2(d), it can be concluded that the modulation of energy-dependent RPTD mainly depends on two-photon ionization phase $s_{2,2}$, rather than on single-photon ionization phase $s_{1,-1}$.

As shown by Fig. 3(a), the population of ground state has dropped to 0.97, 0.75, 0.21, and 0.16 after the first pulse ends for 1, 10, 50, and 100 TW/cm^2, respectively, indicating that the ionization process enters into the nonperturbative regime when the laser intensity is larger than 50 TW/cm^2. Similarly, as shown by Fig. 3(b), at higher intensities (50 and 100 TW/cm^2), ac-Stark energy shift of ground state $\delta E_i(t)$ becomes

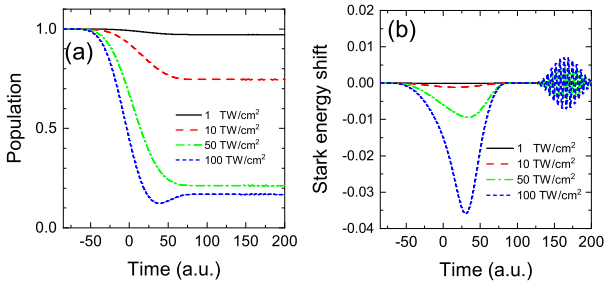


Fig. 3. Time-dependent population $g(t)$ (a) and ac-Stark energy shift $\delta E_i(t)$ (b) at four different laser intensities.

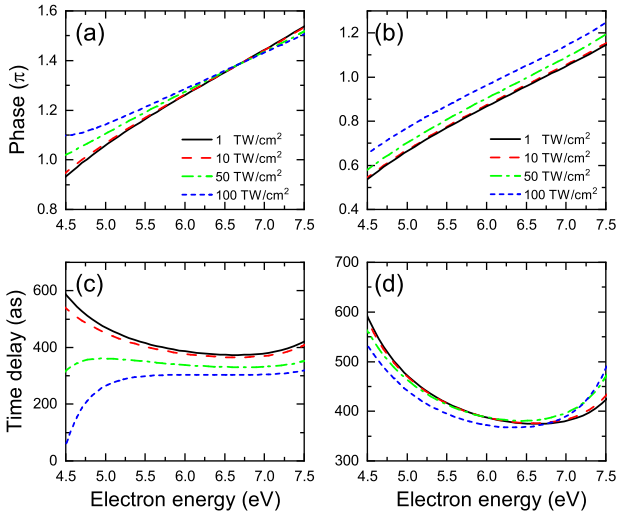


Fig. 4. Two-photon amplitude phase $s_{2,2}$ (top row) and its energy derivative $ds_{2,2}/dE$ (bottom row) obtained by SFNPT with only considering the population depletion (left column) or only considering the Stark energy shift (right column) of ground state.

more pronounced. Hence, the two strong-field effects that the population depletion of the ground-state and its ac-Stark energy shift cannot be ignored in the non-perturbative regime.

In the following part, we employ the SFNPT model to analyze which the strong-field factor dominates in shaping the intensity dependence of $s_{2,2}$. As shown by Fig. 4(a), if the population depletion is only considered, the value of phase $s_{2,2}$ is much smaller than that obtained by the complete TDSE calculations, but its intensity dependence of energy-resolved $s_{2,2}$ is similar to the TDSE-calculated results [see Fig. 2(b)]. Therefore, the energy dependence of $ds_{2,2}/dE$ shown in Fig. 4(c) mimics the behaviors of TDSE results as the intensity increases, demonstrating that the nonperturbative characteristic of RPTD at higher intensity can be well reproduced when only taking the population depletion into account. In contrast, as shown by Fig. 4(b), if we only consider the Stark energy shift, the value of phase $s_{2,2}$ becomes smaller than the case of only considering population, but as the intensity increases, the modulation of each curve is very similar, which leads to its energy derivative being less sensitive to intensity [see Fig. 4(d)]. Therefore, it can be clearly concluded that the population depletion plays a more critical role in shaping the nonperturbative features of RPTD, while the Stark energy shift, although it changes the magnitude of the phase, has little effect on the its energy derivative with the increasing intensity.

It is natural to wonder: which part of the physical process is influenced by the ground state population, such that the derivative of the phase with respect to energy exhibits so pronounced nonperturbative features? From the Eqs. (13) and (14), we know that the two-photon ionization phase $s_{2,2}$ originates from the phase of $\Pi_q(E)$, which denotes the Fourier transform of the laser pulse envelope. In Fig. 5(a) and 5(b), we plot the energy-dependent phase Θ and its energy derivative $d\Theta/dE$ at different intensities, respectively. It can be clearly seen that in the SFNPT model the intensity dependence of phase Θ and its energy derivative $d\Theta/dE$ can well reproduce the nonperturbative features as illustrated by TDSE calculations. When excluding the effect of pulse envelope, i.e, assume that $f(t) = 1$, as shown by Fig. 5(c), the sensitivity of phase Θ to the intensity is significantly suppressed. At lower intensities, Θ in Fig. 5(c) shows an overall increase trend as similar as the results in Fig. 5(a), however, as the intensity increases, the energy dependence of Θ hardly changes. This can also be seen from its energy derivative, as shown by Fig. 5(d), as the intensity increases, although the oscillation of the $d\Theta/dE$ becomes stronger, there is no qualitative change.

Note that the population depletion does more than merely reshape the effective temporal envelope. While $g(t)$ indeed acts as a time-dependent amplitude modulation, its crucial effect is to introduce an "additional complex phase" into $\Pi_q(E)$ beyond a simple envelope rescaling. This arises because $g(t)$ is not a static, symmetric window function: depletion builds up asymmetrically during the pulse (stronger in the trailing edge), thereby breaking the time-reversal symmetry of the integrand in the Fourier transform. A short analytic argument is as follows. In the perturbative limit ($g(t') \equiv 1$) with a symmetric envelope $f(t')$, the Fourier transform is real at resonance, so $\mathrm{Im}[\Pi_q] = 0$.

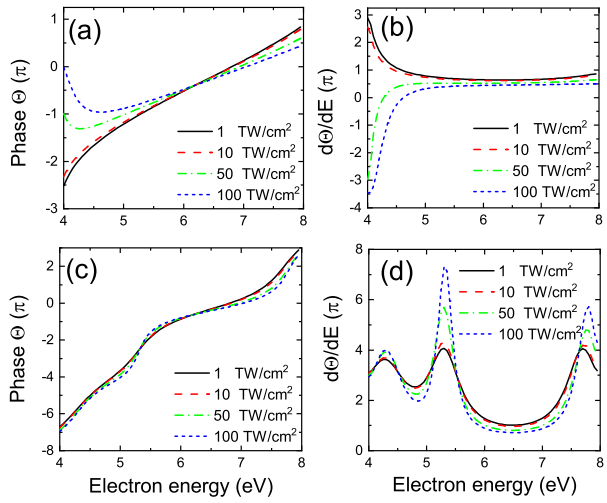


Fig. 5. Energy-dependent the argument of $\Pi_q(E)$, i.e., the phase Θ (left column) and its energy derivative $d\Theta/dE$ (right column) at different intensities for two cases: complete pulse envelope $f(t)$ (top row) and excluding the pulse envelope, i.e., $f(t) = 1$ (bottom row).

When depletion is included, $g(t')$ builds up asymmetrically during the pulse (stronger in the trailing edge), breaking the time-reversal symmetry of the integrand. Consequently, the sine-transform no longer vanishes: $\mathrm{Im}[\Pi_q] \approx \int dt \int^t dt' f(t)f(t')g(t')\sin[\Delta E(t-t')] \neq 0$, where ΔE denotes the energy difference. Because $g(t')$ is intensity-dependent, this non-zero imaginary component acquires an intensity-dependent energy dispersion, directly altering $d[\arg(\Pi_q)]/dE$ and thus producing the nonperturbative behavior of $ds_{2,2}/dE$ shown in Figs. 4 and 5 .

4. Conclusions

In summary, we have presented a theoretical investigation of the intensity-dependent resonant photoionization time delay (RPTD) in atomic hydrogen driven by counter-rotating bicircular two-color XUV laser pulses. By numerically solving the 3D-TDSE and employing SFNPT, we retrieved the energy-resolved RPTD from the relative optical phase corresponding to the maximal asymmetry in photoelectron angular distributions, across a broad intensity range spanning from the perturbative to the nonperturbative regime. Our results reveal a pronounced transition in the energy-dependent behavior of RPTD as the laser intensity increases. In the perturbative regime, the absolute value of RPTD exhibits a smooth monotonic decrease with increasing electron energy. Upon entering the nonperturbative regime, however, this trend is qualitatively altered, and the absolute value of RPTD displays a distinct enhancement as a function of electron energy. By systematically disentangling the roles of strong-field effects within the SFNPT framework, we unambiguously identify the population depletion of the ground state as the dominant mechanism responsible for shaping these nonperturbative characteristics. In contrast, the ac-Stark energy shift of the initial state, while modifying the overall magnitude of the ionization phase, exerts only a minor influence on its energy derivative. Physically, the time-dependent ground-state depletion severely distorts the Fourier transform of the laser pulse envelope, introducing an intensity-dependent imaginary component to the transition amplitude that fundamentally alters the energy derivative of the two-photon ionization phase. These findings clarify the microscopic physical mechanism underlying photoionization time delays in strong-field environments and contribute to a comprehensive understanding of temporal dynamics in attosecond metrology beyond the perturbative limit.

Note that the relative insignificance of the ac-Stark shift on the energy derivative of the two-photon phase is specific to the parameters chosen in this work: relatively short XUV pulses (a few femtoseconds) and near-resonant excitation. Under these conditions, the time-integrated Stark shift remains modest compared to the photon energy, and its effect is largely averaged out when taking the energy derivative. In contrast, for significantly longer pulses or larger detunings from resonance, the ac-Stark shift could accumulate over time and introduce a more pronounced intensity-dependent phase modulation, potentially altering the energy derivative of the transition amplitude. Therefore, our conclusion applies to the short-pulse, near-resonant regime investigated here, and that the dominance of population depletion over Stark shift may weaken for longer pulse durations or larger detunings.

Data availability statement

Data underlying the results presented in this paper are not publicly available at this time but may be obtained from the authors upon reasonable request.

Acknowledgments

We acknowledge Prof. Yan-Jun Chen and Prof. Jing Chen for fruitful discussions. This work is sup-

ported by the Shaanxi Provincial Education Department (Grant No. 24JK0438).

References

[1] Hertz H 1887 *Annalen Physik Chem.* **267**, 983

[2] Einstein A 1905 *Annalen Physik* **17** 132

[3] Wigner E P 1955 *Phys. Rev.* **98** 145

[4] de Carvalho C A A and Nussenzveig H M 2002 *Phys. Rep.* **364** 83

[5] Kheifets A S 2023 *J. Phys. B* **56** 022001

[6] Eckle P, Pfeiffer A N, Cirelli C, Staudte A, Dörner R, Muller H G, Buttiker M and Keller U 2008 *Science* **322** 1525

[7] Goulielmakis E, Loh Z H, Wirth A, *et al.* 2010 *Nature* **466** 739

[8] Kheifets A S and Ivanov I A 2010 *Phys. Rev. Lett.* **105** 233002

[9] Ivanov I A and Kheifets A S 2013 *Phys. Rev. A* **87** 033407

[10] Huppert M, Jordan I, Baykusheva D, von Conta A and Wörner H J 2016 *Phys. Rev. Lett.* **117** 093001

[11] Ma Y Z, Ni H C and Wu J 2024 *Chin. Phys. B* **33** 013201

[12] Itatani J, Quéré F, Yudin G L, Ivanov M Yu, Krausz F and Corkum P B 2002 *Phys. Rev. Lett.* **88** 173903

[13] Schultze M, Fieß M, Karpowicz N, Gagnon J, Korbman M, Hofstetter M, Neppl S, Cavalieri A L, Komninos Y, Mercouris T, Nicolaides C A, Pazourek R, Nagele S, Feist J, Burgdörfer J, Azzeer A M, Ernstorfer R, Kienberger R, Kleineberg U, Goulielmakis E, Krausz F and Yakovlev V S 2010 *Science* **328** 1658

[14] Ortmann L and Landsman A 2024 *Rep. Prog. Phys.* **87** 086401

[15] Paul P M, Toma E S, Breger P, Mullot G, Augé F, Balcou P, Muller H G and Agostini P 2001 *Science* **292** 1689

[16] Klünder K, Dahlström J M, Gisselbrecht M, Fordell T, Swoboda M, Guénot D, Johnsson P, Caillat J, Mauritsson J, Maquet A, Taïeb R and L'Huillier A 2011 *Phys. Rev. Lett.* **106** 143002

[17] You D, Ueda K, Gryzlova E V, *et al.* 2020 *Phys. Rev. X* **10** 031070

[18] Liu M Q, Wang X Q, Jia L J, Yan P G and Jiang W C 2023 *Phys. Rev. A* **108** 013102

[19] Pazourek R, Nagele S and Burgdörfer J 2015 *Rev. Mod. Phys.* **87** 765

[20] Wei C L and Zhao X 2019 *Chin. Phys. B* **28** 013201

[21] Gruson V, Barreau L, Jiménez-Galan Á, Risoud F, Caillat J, Maquet A, Carré B, Lepetit F, Hergott J F, Ruchon T, Argenti L, Taïeb R, Martín F and Salières P 2016 *Science* **354** 734

[22] Song X H, Shi G L, Zhang G J, Xu J W, Lin C, Chen J and Yang W F 2018 *Phys. Rev. Lett.* **121** 103201

[23] Tong J, Liu X, Dong W, Jiang W, Zhu M, Xu Y, Zuo Z, Lu P, Gong X, Song X, Yang W and Wu J 2022 *Phys. Rev. Lett.* **129** 173201

[24] Kheifets A S 2025 *J. Phys. B* **58** 072001

[25] Krausz F and Ivanov M 2009 *Rev. Mod. Phys.* **81** 163

[26] Ngoko Djiokap J M 2021 *Phys. Rev. A* **104** 013115

[27] Donsa S, Douguet N, Burgdörfer J, Březinová I, and Argenti L 2019 *Phys. Rev. Lett.* **123** 133203

[28] Vismarra F, Fernández-Galán M, Mocci D, *et al.* 2024 *Light: Sci. Appl.* **13** 197

[29] Richter F, Saalmann U, Allaria E, *et al.* 2024 *Nature* **636** 337

[30] Wang X W, Xiao F, Wang J C, Wang L, Zhang B, Liu J L, Zhao J and Zhao Z X 2024 *Ultrafast Sci.* **4** 0080

[31] Wu L L, Jiang W C and Peng L Y 2024 *Chin. Phys. B* **33** 074204

[32] Cao Y, Shu Z, Tian D W and Hao X L 2026 *Chin. Phys. B* **35** 064210

[33] Liu M Q, Khan S U, Wang X Q, Yan P G and Jiang W C 2022 *New J. Phys.* **24** 093019

[34] Zhao X Y, Liu M Q and Chen Y J 2026 *Opt. Express* **34** 5501

[35] Arbó D G, Lemell C, Nagele S, Camus N, Fechner L, Krupp A, Pfeifer T, López S D, Moshammer R and Burgdörfer J 2015 *Phys. Rev. A* **92** 023402

[36] Rescigno T N and McCurdy C W 2000 *Phys. Rev. A* **62** 032706

[37] Jiang W C and Tian X Q 2017 *Opt. Express* **25** 26832

[38] Tong X M, Hino K and Toshima N 2006 *Phys. Rev. A* **74** 031405

[39] Su J, Ni H C, Jaroń-Becker A and Becker A 2014 *Phys. Rev. Lett.* **113** 263002